Mesoscale gravity wave variances from AMSU-A radiances

Dong L. Wu
Jet Propulsion Laboratory, California Institute of Technology, Pasadena, California, USA

Received 22 January 2004; revised 12 April 2004; accepted 3 June 2004; published XX Month 2004.

[1] A variance analysis technique is developed here to extract gravity wave (GW) induced temperature fluctuations from NOAA AMSU-A (Advanced Microwave Sounding Unit-A) radiance measurements. By carefully removing the instrument/measurement noise, the algorithm can produce reliable GW variances with the minimum detectable value as small as 0.1 K^2. Preliminary analyses with AMSU-A data show GW variance maps in the stratosphere have very similar distributions to those found with the UARS MLS (Upper Atmosphere Research Satellite Microwave Limb Sounder). However, the AMSU-A offers better horizontal and temporal resolution for observing regional GW variability, such as activity over sub-Antarctic islands. *INDEX TERMS:* 0350 Atmospheric Composition and Structure: Pressure, density, and temperature; 0341 Atmospheric Composition and Structure: Middle atmosphere—constituent transport and chemistry (3334); 1640 Global Change: Remote sensing. **Citation:** Wu, D. L., (2004), Mesoscale gravity wave variances from AMSU-A radiances, *Geophys. Res. Lett.*, *31*, LXXXXX, doi:10.1029/2004GL019562.

1. Introduction

[2] Gravity wave (GW) processes play an important role in the atmospheric circulation, thermal structure and variability on both global and regional scales. Both short-term weather forecast and long-term climate prediction depend on the understanding of these processes, but their effects are not well represented in global numerical weather prediction (NWP) and climate general circulation models (GCMs). Wave drags in large-scale models from these mesoscale/small-scale processes have been treated coarsely with sub-grid-scale parameterizations, which is a major source of uncertainties in model predictability and reliability [e.g., *Fritts and Alexander*, 2003].

[3] Lack of observational constraints on wave properties has been a primary limitation on developing and verifying GW parameterization. Partly because of wave complexities, it is difficult to obtain a complete view of these processes with a single instrument/technique. Radiosonde, lidar, radar, and rocket measurements generally provide good vertical resolutions [e.g., *Allen and Vincent*, 1995; *Wilson et al.*, 1991; *Fukao et al.*, 1994; *Hirota and Niki*, 1985], whereas satellite measurements can yield global coverage of GW activity [e.g., *Fetzer and Gille*, 1994; *Wu and Waters*, 1996; *Dewan et al.*, 1998; *Eckermann and Preusse*, 1999; *Tsuda et al.*, 2000].

[4] GW distribution and variability has been better understood with recent observations from the Microwave Limb Sounder (MLS) on Upper Atmosphere Research Satellite (UARS) [*Wu and Waters*, 1996; *McLandress et al.*, 2000; *Jiang et al.*, 2002]. This passive microwave instrument offers good reliability and stability to detect weak air temperature fluctuations, and ability to map global GW activity. GW variances observed by MLS are found to correlate well with jetstream, deep convection and topography [*McLandress et al.*, 2000; *Jiang et al.*, 2002].

[5] This paper extends the GW variance analysis to the Advanced Microwave Sounding Unit-A (AMSU-A), a passive nadir-viewing microwave sensor on NOAA operational satellites. Compared to MLS, AMSU-A has advantages for better horizontal coverage and for a longer data record. AMSU-A data cover altitudes between the surface to ~2 hPa. Based on the MLS algorithm, a GW variance method is developed here for the AMSU-A radiances and a comparison of MLS and AMSU-A GW maps is made in the end of the paper.

2. AMSU-A Radiances and Variance Analysis

[6] The AMSU-A is a 15-channel nadir sounding instrument with a cross-track swath of ~2,300 km. There are four AMSU instruments currently in operation: three on NOAA N15 (since May 1998), N16 (since September 2000) and N17 (since June 2002) satellites, and one on NASA Aqua satellite. The AMSU-A radiances used in this study are all from the NOAA polar-orbiting satellites that have ~102 min orbiting period and ~7.4 km/s velocity. Only upper air channels (9–14) are used here to avoid possible contaminations from cloud scattering or surface emission.

[7] An AMSU-A scan has 30 FOVs distributed symmetrically about nadir (Figure 1). Each measurement has 0.165 sec integration time and radiometric calibration is performed twice in a scan cycle (8 sec). The half power beamwidth (HPBW) of channels 9–14 is ~3.5° according to the calibration data by *Mo* [1999]. The instrument beamwidth produces footprint sizes of ~50 km near nadir and ~110 km for the outermost beam at scan angle 48.3° from nadir. As shown in Figure 1, the temperature weighting function of this FOV peaks at a higher altitude than those near nadir because of a longer path length. At slant views the two-dimensional (2D) weighting functions become slightly asymmetric about the local zenith as a result of antenna (horizontal) and radiative transfer (vertical) smearing, skewed toward the line-of-sight (LOS) direction. The 2D weighting function asymmetry increases as the instrument FOV decreases, making the radiance variance more sensitive to wave structures and propagation directions. In the UARS MLS case, the beamwidth is ~0.2° and large radiance variance differences were found between ascending and descending orbits [e.g., *McLandress et al.*, 2000].

[8] AMSU-A radiances exhibit an unexpected cross-track asymmetry about the nadir [*Goldberg et al.*, 2001; *Mo*,

0094-8276/04/2004GL019562$05.00

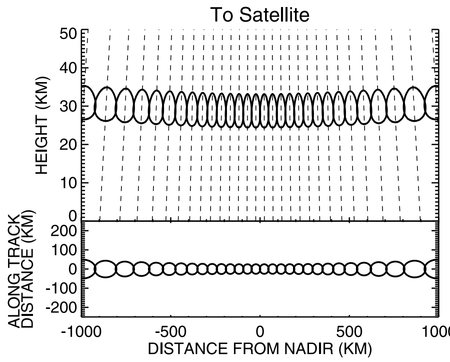

Figure 1. Two-dimensional (2D) AMSU temperature weighting functions (top) and FOV footprints (bottom), calculated using a simple radiative transfer model that includes FOV convolution. Contours represent the half power width of the weighting functions where dashed straight lines represent LOS in each FOV.

1999]. To analyze the AMSU-A radiances, I first remove the systematic scan-angle dependence by fitting the radiances T_b to a polynomial of scan angle θ, given by

$$\widetilde{T}_b(\theta) = a_0 + a_1\theta + a_2\theta^2 + a_3\theta^3 \qquad (1)$$

where a_i are the fitting coefficients and $\widetilde{T}_b(\theta)$ are the fitted radiances. The fitting (1) is applied to a half (15 FOVs on the same side of the track) of the scan at a time. The radiance residual, $\Delta\widetilde{T}_b(\theta) \equiv T_b(\theta) - \widetilde{T}_b(\theta)$, are normally <~0.01 K for no-wave conditions (Figure 2).

[9] However, the averaged radiance residuals from the real data are much larger (0.05–0.2 K) than expected. An example for channel 13 is shown in Figure 3, where these FOV biases are comparable to the specified instrument accuracy. These biases vary somewhat with frequency and satellite but little with latitude and time. Between equatorial (small atmospheric variability) and polar (large atmospheric variability) regions, the deduced biases may differ by <0.02 K.

[10] For GW variance analysis, these radiance biases are significant and must be removed. They are estimated empirically by averaging the radiance residuals obtained in the equatorial region (where atmospheric variability is low). Because short-scale atmospheric variability is unlikely to be coherent on a global scale, the averaged residuals can sufficiently reduce random atmospheric fluctuations and yield the systematic instrument biases. These empirically-determined biases are then subtracted from the radiances in each scan to give "unbiased" radiance residuals, i.e., $\Delta T'_b(\theta) \equiv \Delta\widetilde{T}_b(\theta) - \Delta\widetilde{T}_b(\theta)$ where $\Delta\widetilde{T}_b(\theta)$ is the derived bias as a function of scan angle and frequency channel.

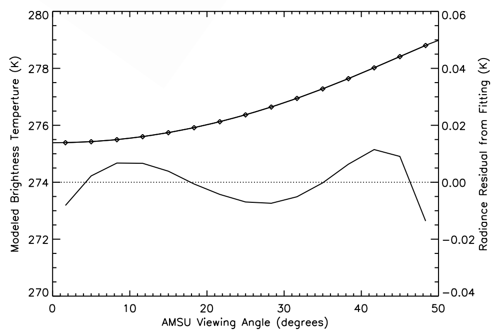

Figure 2. Modeled AMSU-A radiances (symbol) for a no-wave atmosphere and the radiance residuals from fitting (1) as a function of viewing angle. The line through the symbols depicts the fitted function (1).

[11] The next step is to apply a linear fit to the unbiased radiance residuals $\Delta T'_b$ to truncate large-scale perturbations. This truncation is similar to that used in the MLS analysis [*Wu and Waters*, 1996] for removing linear and large-scale wave components. For the AMSU-A analysis, the single-scale radiance residuals are divided into six groups of five for the linear fit, namely,

$$\Delta\hat{T}_b(\theta) = b_0 + b_1\theta \qquad (2)$$

where b_0 and b_1 are the fitting coefficients. The residuals $\Delta\hat{T}_b(\theta) - \Delta T'_b(\theta)$ from the linear fit are used to compute variance $\hat{\sigma}^2$, which is defined by

$$\hat{\sigma}(\theta)^2 \equiv \frac{15}{11} \bullet \frac{5}{3}\left\{\Delta\hat{T}_b(\theta) - \Delta T'_b(\theta)\right\}^2 \qquad (3)$$

where $\frac{15}{11}$ and $\frac{5}{3}$ are the normalization factors (reduction in degrees of freedom) associated with fittings (1) and (2), respectively. This deduced radiance variance has wave power cutoff at a horizontal wavelength of ~250 km for near-nadir FOVs and ~360 km for near-limb FOVs. For MLS limb-tracking data, the cutoff wavelength is somewhat shorter (~100 km) [*Wu and Waters*, 1997].

[12] The radiance variance $\hat{\sigma}^2$ estimated from a single scan may fluctuate, which must be averaged in order to detect weak variances. As shown by *Wu and Waters* [1997], uncertainties in $\hat{\sigma}^2$ is proportional to the truth σ^2

$$\left|\hat{\sigma}^2 - \sigma^2\right| \approx \sqrt{2/M}\sigma^2 \qquad (4)$$

where M is the number of independent measurements for σ^2. In this study, data from N15, N16, and N17 satellites are

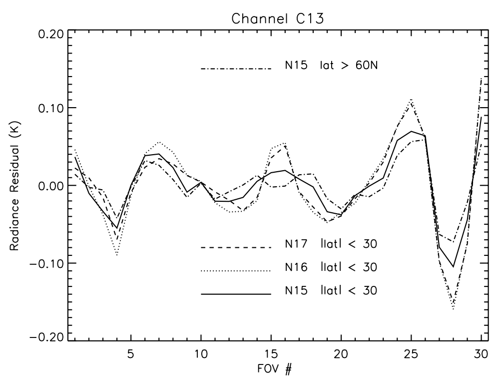

Figure 3. Systematic radiance biases for AMSU-A channel 13 where the scan-angle dependence is removed and the data are averaged for 30°S–30°N during January–September 2003. There are slight differences among N15, N16, and N17 residuals. The cause(s) of these residuals is unclear but spillovers from the antenna side lobes are capable of producing systematic biases with this magnitude [*Mo*, 1999].

Table 1. AMSU-A Instrument Noise for Channels 9–14

Channel Number	Pressure of Weighting Function Peak[a] (hPa)	Measured Noise[b] (K)	Precision Estimated in This Work (K)		
			N15	N16	N17
9	~80	0.24	0.16	0.15	0.15
10	~50	0.25	0.20	0.20	0.20
11	~25	0.28	0.23[c]	0.23	0.23
12	~10	0.40	0.33	0.35	0.35
13	~5	0.54	0.47	0.49	0.50
14	~2.5	0.91	0.79[c]	0.81	0.82

[a]Corresponding to the weighting function of the outermost viewing angles.
[b]From *Goldberg et al.* [2001].
[c]From the early period of N15 operation.

used in averaging and sufficient to produce reliable GW variance maps on a 0.5° × 0.5° grid. With the three satellites, each grid box typically has 24 samples in a month in the equatorial region and 36 in the polar region, and the noise floor can be reduced by factors of 3–4 to <0.15 K^2 for channel 13.

[13] As suggested by *Wu and Waters* [1996], the radiance variance may be interpreted as the sum of atmospheric variance σ_A^2 and instrument variance σ_I^2, namely

$$\sigma^2 = \sigma_A^2 + \sigma_I^2 + \varepsilon \tag{5}$$

where ε represents additional measurement error not accounted by the fittings. This extra component is normally very small compared to the first two. The instrument noise σ_I^2 can be frequency-dependent but is a random component and stable in general throughout the entire mission. Although it was measured before launch, more accurate estimates can be obtained from the real data. A method for noise estimation from flight data was described by *Wu and Waters* [1996] for MLS, using averages of minimum variances in monthly zonal means. Table 1 lists the AMSU-A noise estimated with this method for N15, N16, and N17 satellites. The estimated values for AMSU-A noise/precision show little month-to-month variations and appear slightly smaller than those previously measured.

[14] The atmospheric component σ_A^2, hereafter referred to as GW variance, is mostly induced by GW temperature fluctuations. Roughly speaking, the AMSU-A variances are contributed mostly from waves of horizontal wavelengths between 50–250 km for near-nadir cases (100–400 km for near-limb cases) and vertical wavelengths >10 km. The horizontal wavelengths are determined by the FOV size (at short scales) and the truncation length used in fitting (3) (at large scales). The sensitivity reduces sharply for waves with vertical wavelengths <~10 km, as a result of vertical smearing by the temperature weighting functions.

3. Preliminary Results

[15] GW variance maps for the June–August period are compared in Figure 4 where AMSU-A data are obtained in 2003 from channel 13 (~37 km) and MLS data are from 1991–1994 and channel 3 (~38 km). The most prominent features in common are the enhancements over the southern Andes and Antarctic Peninsula, which was previously investigated in detail with UARS MLS and radiosonde data [*McLandress et al.*, 2000; *Jiang et al.*, 2002; *Wu and Jiang*, 2002]. Due to coarse sampling, MLS variances need to be averaged with a longer observing period and on larger grid boxes than AMSU-A data. Thus, in the MLS map many small localized features seen in the AMSU-A observations may have been smeared but the broad patterns over the southern Andes, Antarctic Peninsula, and South Georgia Island remain very similar in both observations.

[16] The AMSU-A observations confirm the well-correlated enhancement along the stratospheric jetstream at latitudes between 40°S and 70°S, 1000–2000 km away from the Antarctic rim, and reveal many detailed patterns that seem related to sub-Antarctic islands, including South Georgia, Prince Edward Islands, Kerguelen Islands, and Heard Islands. Variances associated with the near-limb FOVs are generally greater than those from near-nadir groups, the latter gives better horizontal resolution and hence sharper maps. The enhancements over New Zealand and Tasmania, Australia are further evidence of topography-related wave activity. The variances over New Zealand are weak and blurred in the MLS observations. Conversely, the enhancement near (150°W, 60°S) in the AMSU-A maps seems not to be associated with any islands. It appears only

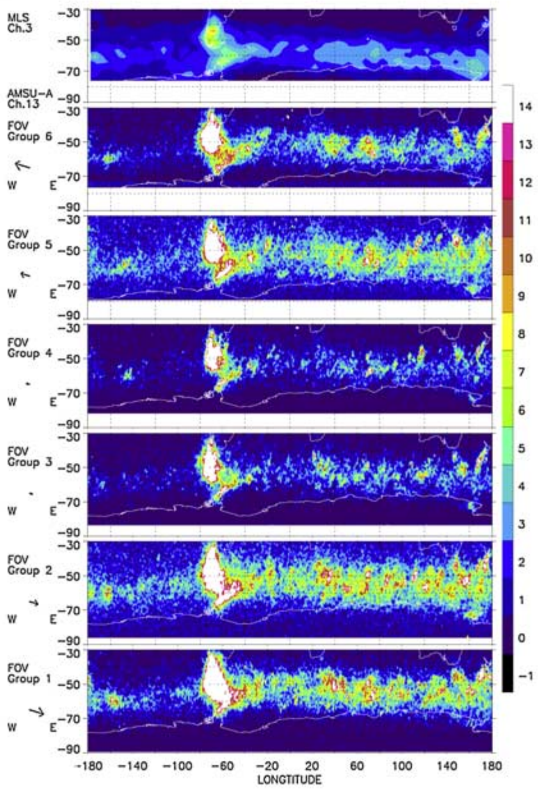

Figure 4. GW variance maps in (−180°, 180°) longitude and (30°S, 90°S) latitude for June–August. The MLS map is on a 5° × 10° latitude-longitude grid and averaged with both ascending and descending data during 1991–1994. The AMSU-A maps are produced on 0.5° × 0.5° grid for descending orbits, and the projected pointing for each FOV group is indicated by the arrow on the right. The MLS and AMSU-A color scales are in 0.004 K^2 and 0.04 K^2, respectively.

significantly in the two near-limb maps and becomes almost absent in the near-nadir maps. It occurs in August and September 2003 but not in June and July 2003. These new GW features and their variations require further theoretical and experimental studies to verify and understand. There are noticeable differences in AMSU-A variances between from group 1 and from group 6. These maps have the same viewing angle but different pointing (east-west) directions. Group 1 map shows average variances of $\sim$2 K^2 over the southern Andes and $\sim$0.6 K^2 over New Zealand, whereas the group 6 variances are only half of those. The variance differences between groups 1 and 6 are significant ($\sim$0.12 K^2 for the 95% significance), likely due to effects of the convolution of GWs with the 3-D instrument weighting functions. Viewing geometry and FOV size are the key factors for interpreting the differences seen between AMSU-A and MLS GW variance maps. MLS has a FOV beamwidth of 0.2° and viewing angle of $\sim$66° from nadir, compared to 3.5° and 48° for AMSU-A. Shallow viewing angles like MLS have better sensitivity to waves with large ratios of vertical/horizontal phase speeds; whereas deep viewing angles like AMSU-A near-nadir FOVs are better for the small ratios (or steep phase fronts). More quantitative studies with the variances require full consideration of the instrument visibility function to atmospheric waves [*Alexander*, 1998; *McLandress et al.*, 2000; *Jiang et al.*, 2004].

4. Summary

[17] This paper describes a variance analysis to extract GW variances from AMSU-A radiance measurements. These GW variances are contributed mostly by mesoscale waves with horizontal wavelengths between 50–200 km and vertical wavelengths >10 km. Multiple AMSU-A channels are used to map GW activities at altitude layers between 80 and 2 hPa, which is an important region for GW generation and propagation. The preliminary results from the radiance variance analysis yield many interesting new features in global GW activity. The channel 13 maps reveal the similar distribution of wave activity to the MLS observations for the June–August period. The most prominent stratospheric GW features are located over the southern Andes and Antarctic Peninsula. The AMSU-A variances from near-nadir FOVs, despite weak amplitude, has the best horizontal resolution to pinpoint the wave sources and their collocation with topography. The analysis also shows that the AMSU-A sampling from N15, N16 and N17 satellites together provide sufficient data for making global GW variance maps on a monthly or even weekly basis. Since GW processes are often associated with broad power spectra, joint observations with nadir (e.g., AMSU) and limb (e.g., MLS and occultation) techniques can provide a more complete view of the full spectrum of these stratospheric waves.

[18] **Acknowledgments.** This work was performed at the Jet Propulsion Laboratory, California Institute of Technology, under contract with NASA. The supports from NASA ACMAP program and from the MLS project are acknowledged. The author thanks Drs. Robert Jarnot, Stephen Eckermann and Jonathan Jiang for valuable discussions on instrument calibration and gravity wave analyses, and people who helped making the AMSU data available for this study, especially, Sherry Harrison at Marshall Space Flight Center, Stan Kidder at Cooperative Institute for Research in the Atmosphere, Zhaohui Cheng at NOAA, and the NOAA Satellite Active Archive center.

References

Alexander, M. J. (1998), Interpretations of observed climatological patterns in stratospheric gravity wave variance, *J. Geophys. Res.*, *103*, 8627–8640.

Allen, S. J., and R. A. Vincent (1995), Gravity wave activity in the lower atmosphere: Seasonal and latitudinal variations, *J. Geophys. Res.*, *100*, 1327–1350.

Dewan, E. M., R. H. Picard, R. R. O'Neil, H. A. Gardiner, J. Gibson, J. D. Mill, E. Richards, M. Kendra, and W. O. Gallery (1998), MSX satellite observations of thunderstorm-generated gravity waves in mid-wave infrared images of the upper stratosphere, *Geophys. Res. Lett.*, *25*, 939–942.

Eckermann, S. D., and P. Preusse (1999), Global measurements of stratospheric mountain waves from space, *Science*, *286*, 1534–1537.

Fetzer, E. J., and J. C. Gille (1994), Gravity wave variance in LIMS temperatures. Part I: Variability and comparison with background winds, *J. Atmos. Sci.*, *51*, 2461–2483.

Fritts, D. C., and M. J. Alexander (2003), Gravity wave dynamics and effects in the middle atmosphere, *Rev. Geophys.*, *41*(1), 1003, doi:10.1029/2001RG000106.

Fukao, S., et al. (1994), Seasonal variability of vertical eddy diffusivity in the middle atmosphere: 1. Three-year observations by the middle and upper atmosphere radar, *J. Geophys. Res.*, *99*, 18,973–18,987.

Goldberg, M. D., D. S. Crosby, and L. Zhou (2001), The limb adjustment of AMSU-A observations: Methodology and validation, *J. Appl. Meteorol.*, *40*, 70–83.

Hirota, I., and T. Niki (1985), A statistical study of inertia-gravity waves in the middle atmosphere, *J. Meteorol. Soc. Jpn.*, *63*, 1055–1066.

Jiang, J. H., D. L. Wu, and S. D. Eckermann (2002), Upper Atmosphere Research Satellite (UARS) MLS observation of mountain waves over the Andes, *J. Geophys. Res.*, *107*(D20), 8273, doi:10.1029/2002JD002091.

Jiang, J. H., S. D. Eckermann, D. L. Wu, and J. Ma (2004), A search for mountain waves in MLS stratospheric limb radiances from the winter Northern Hemisphere: Data analysis and global mountain wave modeling, *J. Geophys. Res.*, *109*, D03107, doi:10.1029/2003JD003974.

McLandress, C., M. J. Alexander, and D. L. Wu (2000), Microwave limb sounder observations of gravity waves in the stratosphere: A climatology and interpretation, *J. Geophys. Res.*, *105*, 1947–1967.

Mo, T. (1999), AMSU-A antenna pattern corrections, *IEEE Trans. Geosci. Remote Sens.*, *37*, 103–112.

Tsuda, T., M. Nishida, C. Rocken, and R. H. Ware (2000), A global morphology of gravity wave activity in the stratosphere revealed by the GPS occultation data (GPS/MET), *J. Geophys. Res.*, *105*, 7257–7273.

Wilson, R., M. L. Chanin, and A. Hauchecorne (1991), Gravity waves in the middle atmosphere observed by Rayleigh Lidar: 2. Climatology, *J. Geophys. Res.*, *96*, 5169–5183.

Wu, D. L., and J. H. Jiang (2002), MLS observations of atmospheric gravity waves over Antarctica, *J. Geophys. Res.*, *107*(D24), 4773, doi:10.1029/2002JD002390.

Wu, D. L., and J. W. Waters (1996), Satellite observations of atmospheric variances: A possible indication of gravity waves, *Geophys. Res. Lett.*, *23*, 3631–3634.

Wu, D. L., and J. W. Waters (1997), Observations of gravity waves with the UARS microwave limb sounder, *Gravity Wave Processes: Their Parameterization in Global Climate Models*, *NATO ASI Ser., Ser. I*, vol. 50, edited by K. Hamilton, pp. 103–120, Springer-Verlag, New York.

D. L. Wu, Jet Propulsion Laboratory, California Institute of Technology, 4800 Oak Drive, Pasadena, CA 91109, USA. (dwu@mls.jpl.nasa.gov)